Int. J. Heat Mass Transfer. Vol. 35, No. 10, pp. 2655–2664, 1992
Printed in Great Britain

0017-9310/92 $5.00 + 0.00

Analysis of heating and evaporation from a liquid film adjacent to a horizontal rotating disk

M. M. RAHMAN and A. FAGHRI
Department of Mechanical and Materials Engineering, Wright State University, Dayton, OH 45435, U.S.A.

(*Received* 10 *June* 1991 *and in final form* 30 *September* 1991)

Abstract—The processes of heating and evaporation in a thin liquid film adjacent to a horizontal disk rotating about a vertical axis at a constant angular velocity is analyzed. The fluid emanates axisymmetrically from a source at the center of the disk and is carried downstream by inertial and centrifugal forces. Closed-form analytical solutions are derived for fully-developed flow and heat transfer. Simplified analyses are also presented for developing heat transfer in a fully-developed flow field. Moreover, a complete three-dimensional numerical simulation of the flow system is carried out using a boundary-fitted moving grid system. The different solution methodologies are compared and the results of a parametric study are presented for a range of Reynolds and Ekman numbers. The rate of heat transfer increased significantly with increasing rotational speed. The Nusselt number defined in terms of film thickness approached a constant value in the fully developed region for the cases of heating and evaporation.

1. INTRODUCTION

THE ANALYSIS of fluid flow and heat transfer in a thin liquid film on a spinning axisymmetric horizontal disk is important for the understanding and design of various heat exchange and chemical processing equipment. Applications include wire and fiber coating, food stuff processing, reactor fluidization, transpiration cooling, etc. The present study was primarily motivated by the concept of spaced-based heat and mass transfer equipment using centrifugally-driven thin liquid films. This kind of rotating system is expected to be very useful in a microgravity environment where the centrifugal body force can be an effective driving mechanism for thinning the film to promote a high rate of heat transfer.

Most earlier studies related to heat transfer in thin films were done for falling film systems where the gravitational body force was the primary mechanism to drive the flow. The laminar, wavy-laminar and turbulent flows were studied, among others, by Seban and Faghri [1–3]. Heat transfer to a thin liquid film adjacent to a rotating surface was considered in connection with condensation and evaporation. Sparrow and Gregg [4] developed an analytical solution for the condensation of saturated vapor on the surface of a horizontal rotating disk. The governing equations for the conservation of mass, momentum and energy were simplified using a similarity transformation and then integrated numerically. Butuzov and Rifert [5] presented a closed-form solution for evaporation from a rotating surface using a basic balance of centrifugal and friction forces acting on the film.

In all the studies related to falling films or flow over a spinning disk, the inertia of the incoming fluid was neglected in comparison to the gravitational or centrifugal forces to simplify the mathematical model. In a real flow problem, however, the inertia may be significant, particularly near the entrance. This kind of flow system was recently investigated by Thomas *et al.* [6, 7] and Rahman and Faghri [8]. In the study by Thomas *et al.* [6], a one-dimensional numerical solution procedure was developed by integrating the mass and momentum conservation equations across the thickness of the film by assuming a uniform velocity profile, and solving the resulting equation to generate the distribution of film height with radius. An approximate distribution of the heat-transfer coefficient was found by using the integral method and assuming a fully-developed flow. Results were presented for different values of Reynolds and Rossby numbers. Thomas *et al.* [7] presented experimental data for the liquid film height distribution and a photographic study of surface waves at different flow rates and rotational speeds. No measurement of the heat-transfer coefficient was attempted in that study.

Rahman and Faghri [8] developed a complete three-dimensional solution algorithm for fluid flow adjacent to a rotating disk. Computations were performed using a curvilinear boundary-fitted coordinate system. The free surface of the film conformed to one of the boundaries of the computation domain. An iterative solution procedure was developed to determine the free surface height distribution that was dependent on flow rate, angular velocity and other parameters. The computed results agreed very well with experimental measurements of Thomas *et al.* [7]. The main objective of this study was to numerically determine the flow field and associated film height distribution. The computation of the heat transfer rate was attempted for the specific case of an isothermal wall condition.

The objective of the present study is to determine

NOMENCLATURE

E	Ekman number, $v/\omega r^2$
g	gravitational acceleration, $-9.81\mathbf{j}$ [m s^{-2}]
h	heat-transfer coefficient, $q_w/(T_w-T_b)$ for heating, $q_w/(T_w-T_{sat})$ for evaporation [W m^{-2} K^{-1}]
$\mathbf{i}$	unit vector in angular direction
$\mathbf{j}$	unit vector in the direction normal to the plate
$\mathbf{k}$	unit vector in z-direction
K	thermal conductivity [W m^{-1} K^{-1}]
n	coordinate normal to the free surface
$\mathbf{n}$	unit vector normal to the free surface
Nu	Nusselt number, (h/K) $[(v^2/g)^{1/3}]$
Nu^*	Nusselt number in terms of film height, $h\delta/K$
p	static pressure [Pa]
Pr	Prandtl number, v/α
q	heat flux [W m^{-2}]
Q	volumetric flow rate [m^3 s^{-1}]
r	radial coordinate [m]
Re	Reynolds number, $W\delta/v$
t	time [s]
$\mathbf{t}$	unit vector tangential to the free surface
T	temperature [K]
u	velocity in angular direction [m s^{-1}]
v	velocity in the direction normal to the plate [m s^{-1}]
$\mathbf{V}$	velocity vector [m s^{-1}]
w	velocity in the z-direction [m s^{-1}]
W	average velocity along the radius [m s^{-1}]
x	coordinate in angular direction [m]
y	coordinate normal to the plate [m]
Y	dimensionless coordinate normal to the plate, y/δ
z	coordinate in the radial flow direction [m]
Z	radial coordinate defined by equation (14b).

Greek symbols

α	thermal diffusivity [m^2 s^{-1}]
δ	film thickness [m]
δ^+	dimensionless film thickness, δ/r_{in}
v	kinematic viscosity [m^2 s^{-1}]
ξ	dimensionless radial coordinate, r/r_{in}
ρ	density [kg m^{-3}]
$\underline{\tau}$	stress tensor [N m^{-2}]
ψ	dimensionless temperature defined by equation (14a)
ω	angular velocity [rad s^{-1}].

Subscripts

b	mixed-mean (bulk) condition
in	condition at entrance
out	condition at exit
sat	saturation condition
w	condition on solid wall.

heat-transfer coefficients during heating and evaporation in a thin film discharged axisymmetrically on the surface of a uniformly-heated horizontal rotating disk. The free surface computational procedure developed by Rahman and Faghri [8] will be used to perform a parametric study on the effects of the flow rate and rate of rotation. Moreover, simplified analyses will be carried out to develop approximate solutions valid for fully-developed flow and developing heat transfer, as well as closed-form solutions valid for fully-developed flow and heat transfer.

2. ANALYSIS AND COMPUTATION

2.1. *Developing flow and heat transfer*

The computation for the most general condition of developing flow and heat transfer was done using a three-dimensional boundary-fitted curvilinear coordinate system schematically shown in Fig. 1. In this system, the local coordinate lines are directed along lines connecting the centers of the adjacent grid cells. The x-axis is defined in the azimuthal direction, y-axis perpendicular to the plate and z-axis along the radial flow direction. The resolutes of the velocity vector in these three directions are u, v and w, respectively. Due to the axisymmetric nature of the flow and vertical entrance and exit sections, u is always parallel to the plate and v is always perpendicular to the plate. The w component, however, changes its direction along the plate depending on the slope of the free surface. The height of the free surface from the solid wall is denoted by δ, which changes with radial direction. The equations governing the conservation of mass, momentum and energy for steady laminar flow in a thin liquid layer involving a newtonian, constant-property liquid with negligible viscous dissipation and pressure work can be written as

$$\nabla\cdot\mathbf{V}=0 \tag{1}$$

$$\frac{\mathrm{D}\mathbf{V}}{\mathrm{D}t}=-\frac{1}{\rho}\nabla p+v\nabla^2\mathbf{V}+g \tag{2}$$

$$\frac{\mathrm{D}T}{\mathrm{D}t}=\alpha\nabla^2T. \tag{3}$$

The boundary conditions are given by

at $z=r_{in}$:

$$u=v=0,\quad w=W_{in}\left[2\left(\frac{y}{\delta}\right)-\left(\frac{y}{\delta}\right)^2\right],\quad T=T_{in} \tag{4}$$

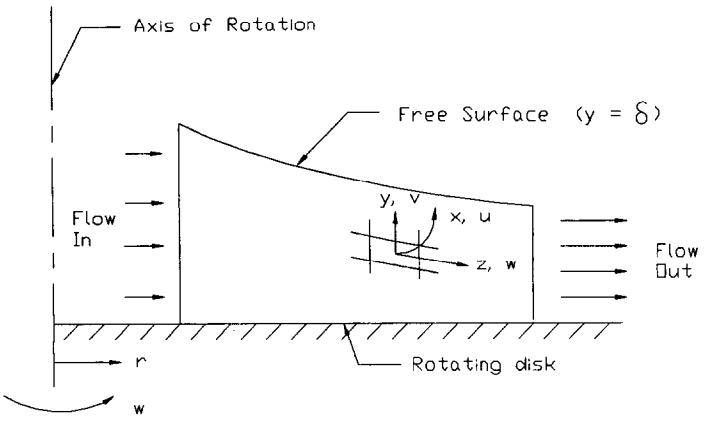

FIG. 1. The flow system and coordinates for computation.

at $z = r_{out}$:

$$\frac{\partial p}{\partial y} = -\rho g, \quad \frac{\partial u}{\partial z} = 0, \quad \frac{\partial w}{\partial z} = 0, \quad \frac{\partial T}{\partial z} = 0 \tag{5}$$

at $y = 0$:

$$u = \omega r, \quad v = w = 0, \quad -K\frac{\partial T}{\partial y} = q_w \tag{6}$$

at $y = \delta$:

$$\frac{d\delta}{dz} = \frac{v}{w}, \quad \underline{\tau}\cdot\mathbf{n} = 0, \quad \underline{\tau}\cdot\mathbf{t} = 0$$

$$\begin{cases} \dfrac{\partial T}{\partial n} = 0, & \text{for heating} \\ T = T_{sat}, & \text{for evaporation.} \end{cases} \tag{7}$$

Since the flow is symmetric about the axis of rotation, there is no variation of velocity or temperature in the angular direction. At the free surface the streamline condition needs to be satisfied, which is appropriate when the rate of evaporation at the free surface is small. The effects of surface tension and interfacial waves at the free surface of the liquid are also assumed to be negligible. Under this condition, the vanishing normal stress conditions can be imposed in a simplified form as a balance between the free surface and ambient pressures. At the entrance plane, the velocity is assumed to be radial with a parabolic profile. At the exit plane, the flow and temperature conditions are usually unknown. These, however, need to be specified for an elliptic problem. It is assumed that the flow and temperature approach a fully-developed condition and the pressure profile is hydrostatic in nature. During the process of simple heating without evaporation, the heat transfer at the free surface is assumed to be negligible, which is valid when the rate of heating at the wall is small. During evaporation, the temperature at the free surface corresponds to the equilibrium saturation temperature. In the present work, we also assumed that the fluid enters the computation domain at the saturation temperature for the case of evaporation. It should also be noted that conduction in the wall (conjugate effect) is also neglected in the present analysis.

The results are presented in dimensionless form for different values of Reynolds and Ekman numbers. Two length scales are appropriate to define the Nusselt number. In the falling film literature, the common length scale is $(\nu^2/g)^{1/3}$, which is used to define Nu in the present study. For any given values of fluid properties and gravitational acceleration, Nu essentially represents the heat-transfer coefficient in dimensionless form. The other length scale is the film thickness δ, which is significant in flows involving a zero gravity environment or rotation. The Nusselt number defined in terms of film thickness is represented here as Nu^*. Since δ varies along the length of the flow, Nu^* presents the combined effects of film height variation and heat or mass transfer rates.

The equations for fluid flow and heat transfer (1)–(3) along with boundary conditions (4)–(7) were solved numerically using a boundary-fitted curvilinear coordinate system illustrated in Fig. 1. The irregular free surface was taken as one of the boundaries of the computational domain, which was pie shaped extending from r_{in} to r_{out} in the radial direction and over a small angle in the angular direction. This prevented both distortion of body-fitted coordinates at larger radii and clustering of grids at smaller radii. The grid cells were generated by an algebraic interpolation between the boundaries of the domain. In general, the cell faces were non-orthogonal to each other. The equations for the conservation of mass, momentum and energy were discretized using the finite-volume formulation [9] by integrating the equations over each cell. The relative importance of convection and diffusion was determined from the magnitude of the local Peclet number and these terms were retained according to the hybrid difference scheme. The flow field was solved by using the SIMPLEST algorithm [10]. The convergence was monitored by checking field values at specific locations as well as the residuals of the governing equations. Acceptable solutions corresponded to invariant spot values to the fourth deci-

mal place as well as residuals of less than 10^{-6} for each equation.

The number of grid cells required for the computation was determined from a series of tests with different combinations of cells in each coordinate direction. In the radial direction computations with 45 and 50 cells yielded identical results. In the direction normal to the plate, 30 cells were found to be adequate. Due to the axisymmetric nature of the flow, only 5 cells with an angular extent of 2.3°/cell were found to be adequate in the azimuthal direction. This provided a total angle of 11.5° for the entire pie-shaped computational domain. Test runs with 3.45°/cell and 2.3°/cell yielded heat-transfer coefficients to within 0.001%. Similarly, runs with 2 cells and 5 cells in the angular direction resulted in heat-transfer coefficients to within 0.0005%. Therefore, the computational domain was divided into $50 \times 30 \times 5$ cells in the radial, axial and azimuthal directions, respectively, by simple algebraic interpolation to generate the grid structure.

For each flow rate and rate of rotation, the location of the free surface was solved by an iterative procedure where only the mass and momentum conservation equations were solved [8]. During the iteration process, the free surface was assumed to be a porous wall through which fluid particles cross depending on the difference between the local and ambient pressures. An outflow took place when the fluid pressure was higher than the ambient and vice versa. Successive improvements of the film height distribution were obtained from the local rate of penetration, and iterations were continued until the rate of penetration became negligible. At this condition, the free surface also formed a streamline. The quantities monitored for convergence were root-sum-square penetration, absolute sum of penetration, and maximum error in flow rate, which were defined as

$$\text{Root-sum-square penetration} = \frac{\sqrt{\sum_{k=1}^{n} (Q_{\text{loss}})_k^2}}{Q_{\text{in}}}$$

$$\text{Absolute sum of penetration} = \frac{\sum_{k=1}^{n} |(Q_{\text{loss}})_k|}{Q_{\text{in}}}$$

$$\text{Maximum error in flow rate} = \frac{|(Q - Q_{\text{in}})|_{\max}}{Q_{\text{in}}}.$$

All these quantities were found to decrease almost monotonically with iterations. The final free surface height distribution always had both absolute sum of penetration and maximum error in flow rate of less than 0.06 and root-sum-square penetration less than 0.02. Once the location of the free surface was determined, the transport equations were solved for that particular free surface height distribution to determine the heat-transfer coefficient distribution.

2.2. *Developing heat transfer in fully-developed flow*

The governing equations presented in the previous section can be greatly simplified only if the most dominant transport mechanisms are retained in the problem, making an analytical solution possible. For the analysis presented here, a cylindrical coordinate system (r–x–y) attached to the center of the disk is used. Since the thickness of the film is small, $v \ll u$ or w, and $\partial/\partial y \gg \partial/\partial r$. Also, the gravitational body force is small compared to the centrifugal force even at a moderate rate of rotation. Therefore, $g \approx 0$, and the pressure everywhere is the same as the ambient pressure leading to $p =$ constant. Under further assumptions of $w \ll u$ and solid-body rotation, $u = \omega r$, which can be realized at large rates of rotation, the momentum balance can be written as

$$\frac{d^2 w}{dy^2} = -\frac{\omega^2 r}{\nu}. \tag{8}$$

This equation can be integrated using the boundary conditions at the wall (at $y = 0$: $w = 0$) and on the free surface (at $y = \delta$: $dw/dy = 0$) to develop an expression for the radial velocity

$$w = \frac{\omega^2 r \delta^2}{2\nu}\left[2\left(\frac{y}{\delta}\right) - \left(\frac{y}{\delta}\right)^2\right]. \tag{9}$$

The average velocity W at any radial location can be determined by integrating the local radial velocity across the thickness of the film

$$W = \frac{\omega^2 r \delta^2}{3\nu}. \tag{10}$$

The film thickness as a function of radius can be calculated by satisfying the conservation of mass at each radial location

$$\delta = \left(\frac{3\nu Q}{2\pi\omega^2 r^2}\right)^{1/3}. \tag{11}$$

For a given flow rate and rate of rotation, equation (11) gives the fully-developed film height distribution and equation (9) presents the corresponding local radial velocity distribution. Equation (11) agrees well with results of Needham and Merkin [11] who studied surface waves using a perturbation technique and obtained the zeroth-order film height under similar assumptions.

Incorporating the assumptions of negligible diffusion in the radial direction and a small velocity across the thickness of the film, the energy equation can be written as

$$w\frac{\partial T}{\partial r} = \alpha\frac{\partial^2 T}{\partial y^2}. \tag{12}$$

Using equations (9)–(11), and writing in terms of non-dimensional variables, this equation can be expressed as

$$(2Y - Y^2)\frac{\partial \psi}{\partial Z} = \frac{\partial^2 \psi}{\partial Y^2} \tag{13}$$

where

$$\psi = \frac{T - T_{in}}{q_w r_{in}/K}, \quad Y = \frac{y}{\delta}, \quad \xi = \frac{r}{r_{in}} \tag{14a}$$

and

$$Z = 0.173 Re_{in}^{-4/3} E_{in}^{-2/3} Pr^{-1}[\xi^{8/3} - 1]. \tag{14b}$$

The boundary conditions (4), (6) and (7) can be expressed in non-dimensional form as

$$\text{at } Z = 0: \quad \psi = 0 \tag{15a}$$

$$\text{at } Y = 0: \quad \frac{\partial \psi}{\partial Y} = -(3)^{1/3} Re_{in}^{1/3} E_{in}^{2/3} \xi^{-2/3} \tag{15b}$$

$$\text{at } Y = 1: \quad \begin{cases} \partial\psi/\partial Y = 0, & \text{for heating} \\ \psi = 0, & \text{for evaporation.} \end{cases} \tag{15c}$$

Note that $T_{in} = T_{sat}$ for the case of evaporation. The reduced parabolic equation (13) along with boundary conditions (15) was solved for the processes of heating and evaporation using a finite-difference method where the solution marched along the Z direction and implicitly solved for the temperature distribution as a function of Y. The mixed-mean (or bulk) temperature at any Z location was calculated as

$$\psi_b = \int_0^1 (2Y - Y^2)\psi \, dY. \tag{16}$$

The distributions of Nu and Nu^* were also calculated from the temperature field.

2.3. *Fully-developed flow and heat transfer*

Closed-form analytical solutions can be developed if the heat transfer is also assumed to be fully-developed in nature. For the case of heating without evaporation, the free surface is approximately adiabatic in nature. Then, for a constant heat flux at the wall,

$$\frac{\partial T}{\partial r} \approx \frac{dT_b}{dr}.$$

Substituting this condition into equation (12) along with the use of equations (9)–(11) gives

$$\frac{\partial^2 T}{\partial y^2} = \frac{3W}{2\alpha}\left[2\left(\frac{y}{\delta}\right) - \left(\frac{y}{\delta}\right)^2\right]\frac{dT_b}{dr}. \tag{17}$$

Integrating this equation twice and using the adiabatic condition on the free surface and wall temperature T_w, which is a function of radius, the temperature distribution is

$$T = T_w - \frac{W\delta^2}{\alpha}\left(\frac{dT_b}{dr}\right)\left[\left(\frac{y}{\delta}\right) - \frac{1}{2}\left(\frac{y}{\delta}\right)^3 + \frac{1}{8}\left(\frac{y}{\delta}\right)^4\right]. \tag{18}$$

Evaluating the bulk temperature from this temperature distribution and relating the bulk temperature variation with surface heat flux from a basic energy balance, the heat-transfer coefficient can be expressed as

$$Nu^* = \frac{35}{17}. \tag{19}$$

When evaporation is present, the temperature at the free surface is the same as the equilibrium saturation temperature. Also, in a fully-developed condition, the heat flux from the wall is entirely used for evaporation and not convected downstream. Equation (12) can then be written as

$$\frac{d^2T}{dy^2} = 0. \tag{20}$$

Solving this equation, along with boundary conditions (6) and (7) at the wall and on the free surface, one obtains

$$Nu^* = 1. \tag{21}$$

Therefore, in a fully-developed condition, Nu^* becomes constant for the cases of heating and evaporation. Since the film height decreases with radius, the actual heat-transfer coefficient increases with radius. Nu is related to Nu^* by the relationship

$$Nu = Nu^* A Re_{in}^{-1/3} E_{in}^{-2/3} \xi^{2/3} \tag{22}$$

where

$$A = \left(\frac{\nu^2}{3gr_{in}^3}\right)^{1/3}.$$

3. DISCUSSION OF RESULTS

The three different solution procedures described in the previous section were used to predict the film height and heat-transfer coefficient distributions during heating and evaporation. The present work has two distinct objectives: to compare results corresponding to these fully-developed and developing flow situations, and to simulate the transport processes numerically for the specific disk unit used by Thomas *et al.* [7] for experimental measurements of film height and flow visualization. The experimental unit consisted of a horizontal disk of 406.4 mm in diameter where water at 20°C was introduced radially through a slot 0.267 mm in height at a radial location of 50.8 mm. The film height distribution along the radius was measured by using a non-obtrusive capacitance probe from 76.2 to 195.6 mm. Twenty sets of experimental data were taken covering flow rates of 7–15 lpm and rotational speeds of 55–300 rpm. The flow was isothermal and no measurement of heat transfer was reported in that effort. The specific experimental runs chosen for numerical simulation (cases 1–6) are listed in Table 1. Prediction of heat transfer could be done for all the experimental conditions. However, some specific cases covering the range of experiments in terms of flow rate and rate of rotation were selected to understand the transport phenomena efficiently with a limited amount of computational efforts. Table 1 also lists some runs (cases 7–9) for which experiments were not performed. The numerical computation of these

Table 1. The specifications of flow parameters for the flow over a rotating disk

Case	Flow rate (lpm)	Rotational speed (rpm)	Reynolds number (Re_{in})	Ekman number (E_{in})
1	15	55	520	3.0×10^{-5}
2	15	100	520	1.7×10^{-5}
3	15	200	520	8.3×10^{-6}
4	15	300	520	5.5×10^{-6}
5	11	100	380	1.7×10^{-5}
6	7	100	240	1.7×10^{-5}
7	3	100	100	1.7×10^{-5}
8	30	100	1040	1.7×10^{-5}
9	15	600	520	2.8×10^{-6}

cases were done to understand the behavior of the flow and transport under an extended range of operating conditions.

The computation was started from a radial location of $r_{in} = 76.2$ mm. This corresponded to the location where experimental measurements were also started. The measured film height at that location corresponded to the inlet film height (δ_{in}) for numerical simulation. For cases 7–9, δ_{in} was assumed to be 0.3 mm, which was approximately an average of the measured height at that location for different flow rates and rates of rotation. The radial velocity profile at the entrance plane was assumed to be parabolic in nature with zero at the wall and maximum at the free surface. The heat flux at the wall was assumed to be $q_w = 1000$ W m^{-2}. The fluid (water) entered the computation domain with a uniform temperature of 10°C. The properties were calculated at an estimated bulk temperature of 20°C. The rate of evaporation was very small compared to the fluid flow rate, so the latent cooling due to evaporation had a negligible influence on heat transfer from the wall.

The results are presented in dimensionless form using Reynolds and Ekman numbers as parameters. Table 1 also lists these parameters. The Reynolds number shows the effects of inertia whereas Ekman number shows the effects of rotation on the fluid transport. In the previous work of Thomas *et al.* [6], Rossby number was used to non-dimensionalize the rotational speed. However, the Ekman number is a better parameter since it is a ratio of viscous resisting force to centrifugal force and therefore is not affected by inertia. Moreover, it has been widely used in rotating and atmospheric flows [12].

Figure 2 shows the variation of film height at $Re_{in} = 520$ for two different Ekman numbers, corresponding to two different rates of rotation. The analytical fully-developed solution, which ignores the effects of inertia and assumes solid-body rotation, predicts a monotonic decrease in film height. The numerical solution, which simulates the flow more exactly, shows an increment of film height at smaller radii, attainment of a peak, and then a gradual reduction in height further downstream. At smaller radii, the order of magnitude of the inertial and viscous forces is comparable to that of the centrifugal force. The frictional resistance from the wall tends to increase the film height at that location. With the increase of radius, however, the inertia effects vanish and the frictional force becomes smaller compared to the centrifugal force. Therefore, the numerical solution approaches the analytical solution at large values of ξ. Figure 2 also shows the variation of dimensionless bulk temperature with radius for both developing flow and for fully-developed flow with developing heat transfer when the disk surface is maintained at a constant heat flux condition and the free surface is adiabatic. As expected, the bulk temperature increases monotonically downstream.

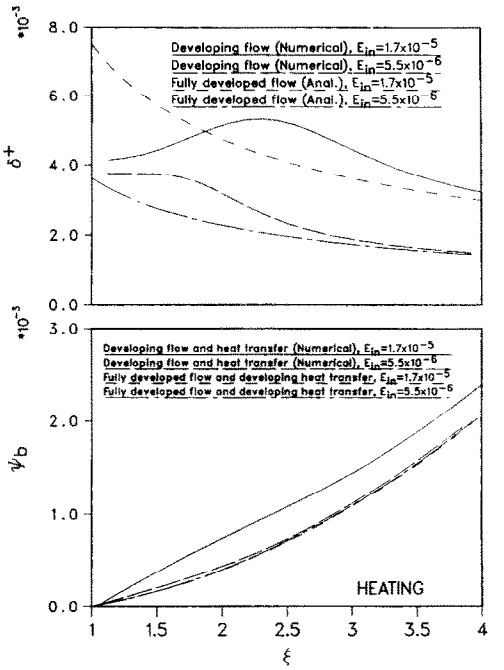

FIG. 2. Comparison of film height variation and bulk temperature for flow over a rotating disk at $Re_{in} = 520$.

Figure 3 shows the variations of Nu and Nu^* for heating from a constant flux wall for the flow and rotation conditions considered in the previous figure. The solutions for developing flow and heat transfer and for developing heat transfer in fully-developed flow approach the fully-developed heat transfer solution where Nu^* becomes constant. This indicates that both flow and heat transfer reach a fully-developed condition within a short distance from the entrance. The heat-transfer coefficient is high near the entrance and decreases downstream due to the development of a thermal boundary layer with the entrance section as the leading edge. The heat-transfer coefficient, however, attains a minimum and increases further downstream due to the increasing centrifugal force at larger radii. The enhancement of the heat-transfer coefficient with centrifugal force is also evident from a comparison of results for two different Ekman numbers. With an increase in rotational speed, the

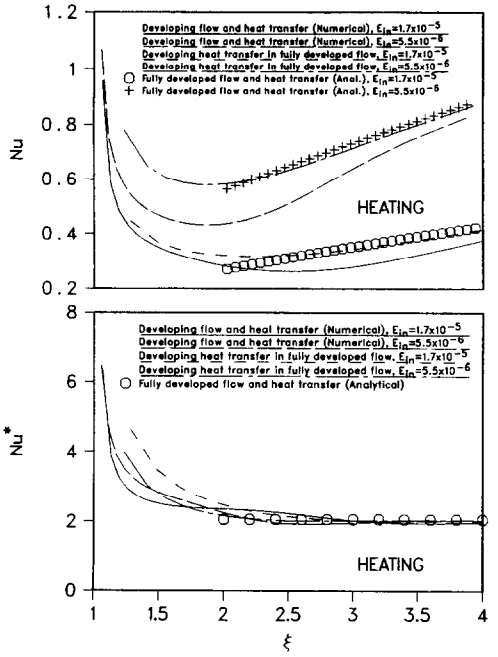

FIG. 3. Comparison of Nusselt number variation for flow over a rotating disk with $Re_{in} = 520$ and simple heating at the disk surface.

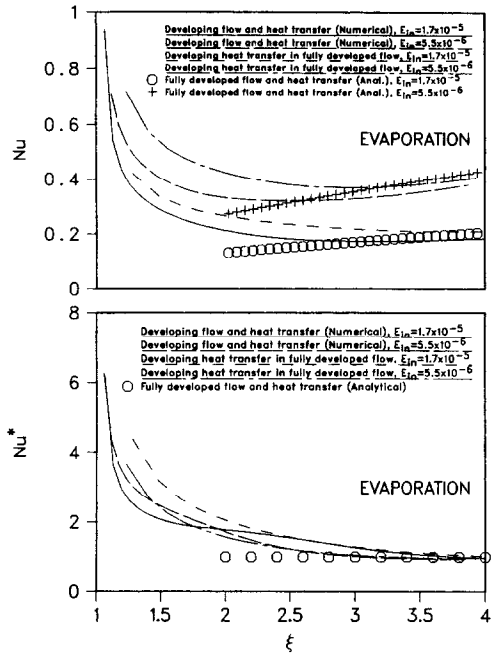

FIG. 4. Comparison of Nusselt number variation for flow over a rotating disk with $Re_{in} = 520$ and evaporation at the free surface.

Ekman number decreases and heat-transfer coefficient increases significantly. By changing the rotational speed from 100 to 300 rpm, a two-fold increase in the overall heat-transfer coefficient is attained. The analytical and numerical predictions of Nu^* compare very well, but Nu does not do so because of the difference between the numerically simulated film height and that estimated from a fully-developed analysis.

The distribution of Nu and Nu^* for the case of evaporation from the free surface for a constant heat flux at the wall is presented in Fig. 4. The solutions corresponding to developing flow and heat transfer and those for fully-developed flow with developing heat transfer approach the fully-developed solution at large radii. For the case of evaporation, the attainment of the fully-developed condition appears to take a larger distance than that for heating without evaporation. The heat-transfer coefficient, which is directly proportional to Nu, decreases downstream from the entrance due to the development of the thermal boundary layer, attains a minimum and then increases downstream where the centrifugal force overcomes the frictional resistance. Since a total development of flow and heat transfer could not be realized within the radius of the disk used by Thomas *et al.* [7], the results shown in Figs. 2–4 were computed for a larger disk, where different possible analytical and numerical approaches could be compared. The numerical solutions corresponding to the experimental system of Thomas *et al.* [7] are presented in Figs. 5–9.

Figure 5 shows the variation of dimensionless film thickness δ^+ and dimensionless bulk temperature ψ_b for the case of heating without evaporation for different combinations of Reynolds and Ekman numbers. The bulk temperature distributions for the case of evaporation are not presented here since the heat-transfer coefficient is defined in terms of the saturation

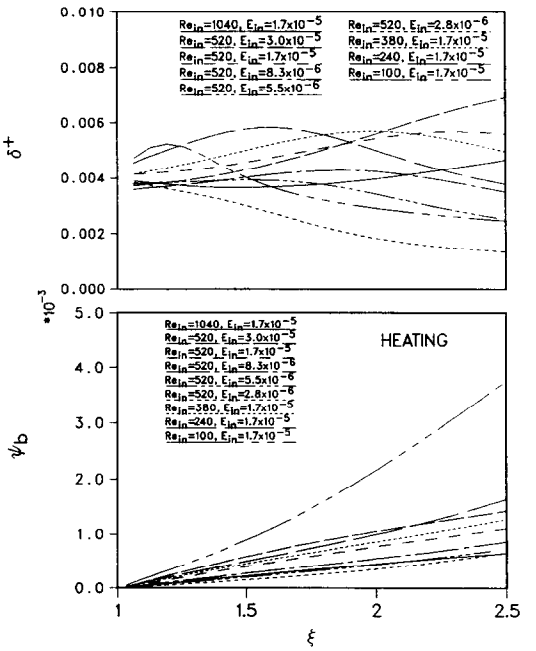

FIG. 5. Numerically predicted film height variation and bulk temperature for developing flow and heat transfer from a rotating disk.

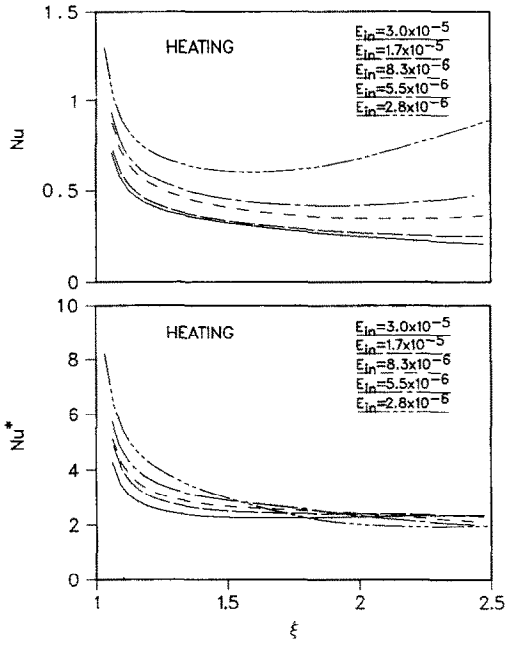

FIG. 6. Numerically predicted Nusselt number variation for developing flow and heat transfer from a rotating disk with $Re_{in} = 520$ and simple heating at the disk surface.

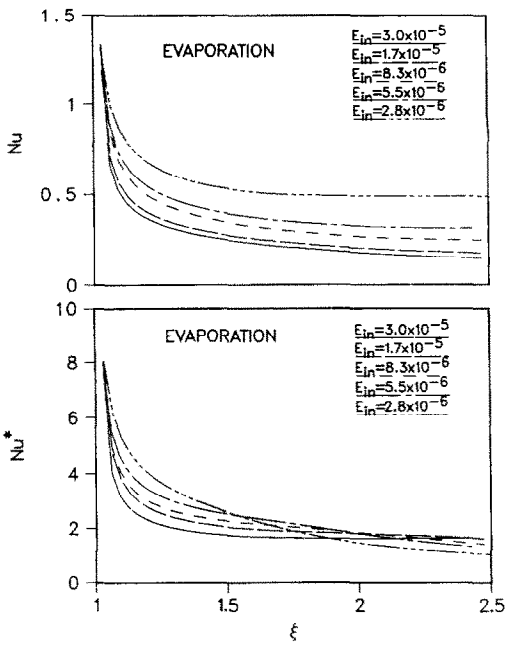

FIG. 8. Numerically predicted Nusselt number variation for developing flow and heat transfer from a rotating disk with $Re_{in} = 520$ and evaporation at the free surface.

temperature. The combinations of Reynolds and Ekman number chosen here correspond to the cases listed in Table 1.

The variation of Nusselt number for the case of simple heating from a constant flux wall are presented in Figs. 6 and 7. Figure 6 shows the effects of Ekman number for $Re_{in} = 520$. At all rates of rotation, both *Nu* and *Nu** are high near the entrance and decrease gradually downstream because of the development of the thermal boundary layer. For the system considered here, at small rotational speeds (i.e. large Ekman numbers), *Nu* monotonically decreases downstream, whereas at larger rotational speeds, *Nu* attains a minimum and increases downstream. This

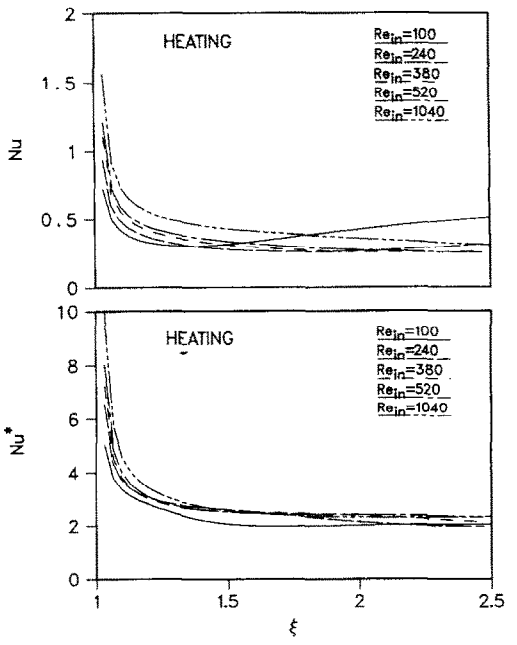

FIG. 7. Numerically predicted Nusselt number variation for developing flow and heat transfer from a rotating disk with $E_{in} = 1.7 \times 10^{-5}$ and simple heating at the disk surface.

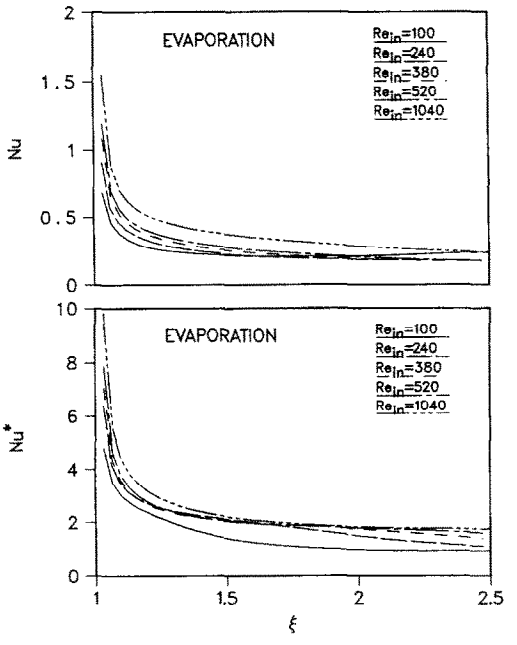

FIG. 9. Numerically predicted Nusselt number variation for developing flow and heat transfer from a rotating disk with $E_{in} = 1.7 \times 10^{-5}$ and evaporation at the free surface.

increment appears to be very significant at an Ekman number of 2.8×10^{-6}. As discussed before, this increment of the heat-transfer coefficient is a result of the centrifugal force that increases the fluid velocity by overcoming the viscous resistance, and causes an augmentation in the convective heat transfer. As expected, the location where the minimum heat transfer is encountered increases with Ekman number. Also, a very significant enhancement of the heat-transfer coefficient is attained with an increase in rotational speed.

Figure 6 also shows the distribution of Nu^* which combines the effects of heat-transfer coefficient and film thickness. At smaller radii, Nu^* increases with decreasing values of Ekman number. However, an opposite trend is seen at larger radial locations. The behavior at smaller ξ is due to the fact that the heat-transfer coefficient is greater at smaller Ekman numbers (larger rates of rotation). With an increase in rotational speed, however, the flow becomes fully-developed at smaller radii and approaches the constant value predicted by the analysis of fully-developed heat transfer more quickly. Therefore, a larger slope is encountered at a smaller value of Ekman number. Also for the disk unit considered here, the heat transfer does not become fully-developed except for the largest rate of rotation.

Figure 7 shows the variation of Nu and Nu^* with Reynolds number at a specific rate of rotation ($E_{in} = 1.7 \times 10^{-5}$). The Reynolds number does not have a very strong effect on the distribution of heat-transfer coefficient. At smaller radii, where the effects of inertia are significant, the heat-transfer coefficient increases with Reynolds number. At large radii, however, a larger heat-transfer coefficient may be obtained even for a smaller flow rate, since inertia effects decrease and the flow is dominated by centrifugal force. For smaller flow rates, the film becomes thinner, and therefore the local velocity next to the wall, which ultimately influences the heat-transfer coefficient, may become larger. It may also be noticed that at a smaller flow rate Nu attains a minimum inside the disk unit and increases further downstream, due to stronger influence of centrifugal force. From Fig. 7, it can also be seen that Nu^* approaches the constant asymptotic value after the initial development of the thermal boundary layer.

The variation of local Nusselt number with Ekman number for the case of evaporation at the free surface while the wall is maintained at a constant heat flux condition is presented in Fig. 8. It appears that the heat-transfer coefficient is very significantly increased with the rate of rotation during the process of evaporation. The decrease of Nu with ξ is caused by the development of the thermal boundary layer. Unlike the case of heating, for the radius and rotational speeds considered here, the heat-transfer coefficient does not attain a minimum within the computation domain. Nu^* shows approximately the same behavior as that for the case of heating without evaporation, but values of the transport coefficients are different. The variation of Nu and Nu^* with Reynolds number for the case of evaporation is shown in Fig. 9. The enhancement of the heat-transfer coefficient with flow rate is seen at most locations on the disk except very close to the exit. Figures 6–9 demonstrate the variation of local heat-transfer coefficients. Considering the average heat-transfer coefficient for the entire disk, it was found that an overall enhancement of heat and mass transfer is attained both with flow rate and rate of rotation.

4. CONCLUSIONS

Numerically computed and analytically predicted results of fluid flow and heat transfer are presented for the free surface flow of a thin liquid film adjacent to a horizontal rotating disk for the case of constant heat flux at the wall. The heat-transfer coefficients were found to decrease gradually from a large value near the entrance due to the development of the thermal boundary layer starting at the entrance section. The heat-transfer coefficient attained a minimum and increased downstream at large radii because of the stronger centrifugal force at that location. A fully-developed condition was attained at large radial locations where Nu^* became constant for the cases of heating and evaporation. The radial location where the fully-developed condition was reached increased with Ekman number, and was found to be greater for the case of evaporation than for the case of heating without evaporation. The effects of flow rate on the enhancement of the heat-transfer coefficient was found to be small. However, a large enhancement of heat and mass transfer was obtained by increasing the rotational speed. This suggests that rotation can be an effective means for the augmentation of heat transfer in equipment designed for operation on earth or in orbit.

REFERENCES

1. R. A. Seban and A. Faghri, Evaporation and heating with turbulent falling liquid films, *ASME J. Heat Transfer* **98**, 315–318 (1976).
2. R. A. Seban and A. Faghri, Wave effects on the transport to falling laminar liquid films, *ASME J. Heat Transfer* **100**, 143–147 (1978).
3. A. Faghri and R. A. Seban, Heat transfer in wavy liquid films, *Int. J. Heat Mass Transfer* **28**, 506–508 (1985).
4. E. M. Sparrow and J. L. Gregg, A theory of rotating condensation, *ASME J. Heat Transfer* **81**, 113–120 (1959).
5. A. I. Butuzov and V. G. Rifert, Heat transfer in evaporation of liquid from a film on a rotating disk, *Heat Transfer—Soviet Res.* **5**, 57–61 (1973).
6. S. Thomas, W. L. Hankey, A. Faghri and T. Swanson, One-dimensional analysis of hydrodynamic and thermal characteristics of thin film flows including the hydraulic jump and rotation, *ASME J. Heat Transfer* **112**, 728–735 (1990).
7. S. Thomas, A. Faghri and W. L. Hankey, Experimental

analysis and flow visualization of a thin liquid film on a stationary and rotating disk, *ASME J. Fluids Engng* **113**, 73–80 (1991).
8. M. M. Rahman and A. Faghri, Numerical simulation of fluid flow and heat transfer in a thin liquid film over a rotating disk, *Int. J. Heat Mass Transfer* **35**, 1441–1453 (1992).
9. S. V. Patankar, *Numerical Heat Transfer and Fluid Flow*. Hemisphere, New York (1980).
10. D. B. Spalding, Mathematical modeling of fluid mechanics, heat transfer and chemical reaction processes, A Lecture Course, CFDU HTS/80/1, Imperial College, London, U.K. (1980).
11. D. J. Needham and J. H. Merkin, The development of nonlinear waves on the surface of a horizontally rotating thin liquid film, *J. Fluid Mech.* **184**, 357–379 (1987).
12. G. K. Batchelor, *An Introduction to Fluid Dynamics*. Cambridge University Press, Cambridge, U.K. (1983).

ANALYSE DU CHAUFFAGE ET DE L'EVAPORATION D'UN FILM LIQUIDE ADJACENT A UN DISQUE HORIZONTAL TOURNANT

Résumé—On analyse les mécanismes de chauffage et de l'évaporation d'un film mince liquide adjacent à un disque horizontal tournant autour d'un axe vertical à vitesse angulaire constante. Le fluide arrive axisymétriquement au centre du disque et il est mû par les forces d'inertie et centrifuges. Des solutions analytiques sont obtenues pour l'écoulement et le transfert de chaleur établis. On présente aussi des analyses simplifiées pour le développement du transfert thermique dans un écoulement établi. Une simulation numérique tridimensionnelle complète est conduite en utilisant un système de grille à frontière mobile. On compare les différentes méthodologies de résolution et les résultats d'une étude paramétrique sont présentés pour un domaine de nombre de Reynolds et d'Ekman. Le flux thermique augmente significativement avec la vitesse de rotation. Le nombre de Nusselt défini sur l'épaisseur du film approche une valeur constante dans la région établie dans les cas du chauffage et de l'évaporation.

BERECHNUNG DER BEHEIZUNG UND VERDAMPFUNG VON EINEM FLÜSSIGKEITSFILM AN EINER WAAGERECHTEN ROTIERENDEN SCHEIBE

Zusammenfassung—Es wird der Vorgang der Beheizung und der Verdampfung in einem dünnen Flüssigkeitsfilm an einer waagerechten Scheibe untersucht, die sich mit konstanter Geschwindigkeit um eine senkrechte Achse dreht. Das Fluid tritt achsensymmetrisch aus einer Quelle in der Scheibenmitte aus und strömt aufgrund von Trägheits- und Zentrifugalkräften nach außen. Für voll ausgebildete Strömung und Wärmeübergang werden geschlossene analytische Lösungen abgeleitet. Für den sich einstellenden Wärmeübergang in einem stationären Strömungsfeld wird eine vereinfachte Berechnung vorgestellt. Darüber hinaus wird unter Verwendung eines an die Grenzen angepaßten beweglichen Rechennetzes eine vollständige dreidimensionale numerische Simulation für die Strömung durchgeführt. Die verschiedenen Lösungsmethoden werden verglichen. Für eine Reihe von Reynolds- und Ekmann-Zahlen werden die Ergebnisse einer Parameterstudie vorgestellt. Der Wärmeübergang verbessert sich spürbar mit zunehmender Rotationsgeschwindigkeit. Die mit der Filmdicke gebildete Nusselt-Zahl erreicht für Beheizung und für Verdampfung im voll ausgebildeten Zustand einen konstanten Wert.

АНАЛИЗ НАГРЕВА И ИСПАРЕНИЯ ЖИДКОЙ ПЛЕНКИ, ПРИЛЕГАЮЩЕЙ К ГОРИЗОНТАЛЬНОМУ ВРАЩАЮЩЕМУСЯ ДИСКУ

Аннотация—Анализируются процессы нагрева и испарения в тонкой жидкой пленке, прилегающей к горизонтальному диску, который вращается относительно вертикальной оси с постоянной угловой скоростью. Жидкость осесимметрично истекает из источника, расположенного в центре диска, и уносится вниз по потоку инерционными и центробежными силами. Получены аналитические выражения для развитых теплопереноса и поля течения. Представлен также упрощенный анализ для устанавливающегося теплопереноса в развитом поле течения. Проводится полное трехмерное численное моделирование течения с помощью адаптивной сетки у границы. Сравниваются различные методики решения, и приводятся результаты параметрического исследования в используемом диапазоне изменений чисел Рейнольдса и Экмана. Интенсивность теплопереноса существенно возрастает с увеличением скорости вращения. При нагреве и испарении число Нуссельта, выраженное через толщину пленки, приближается к постоянному значению в развитой области.